



THE UNIVERSITY *of* EDINBURGH

Edinburgh Research Explorer

## Micro-fabricated caesium vapour cell with 5mm optical path length

**Citation for published version:**

Dyer, T, Ingleby, SJ, Dunare, C, Dodds, K, Lomax, P, Griffin, PF & Riis, E 2022, 'Micro-fabricated caesium vapour cell with 5mm optical path length', *Journal of applied physics*, vol. 132, no. 20, 204401.  
<https://doi.org/10.1063/5.0125490>

**Digital Object Identifier (DOI):**

[10.1063/5.0125490](https://doi.org/10.1063/5.0125490)

**Link:**

[Link to publication record in Edinburgh Research Explorer](#)

**Document Version:**

Peer reviewed version

**Published In:**

Journal of applied physics

**General rights**

Copyright for the publications made accessible via the Edinburgh Research Explorer is retained by the author(s) and / or other copyright owners and it is a condition of accessing these publications that users recognise and abide by the legal requirements associated with these rights.

**Take down policy**

The University of Edinburgh has made every reasonable effort to ensure that Edinburgh Research Explorer content complies with UK legislation. If you believe that the public display of this file breaches copyright please contact [openaccess@ed.ac.uk](mailto:openaccess@ed.ac.uk) providing details, and we will remove access to the work immediately and investigate your claim.



# Micro-fabricated caesium vapour cell with 5 mm optical path length

T. Dyer,<sup>1</sup> S.J. Ingleby,<sup>1</sup> C. Dunare,<sup>2</sup> K. Dodds,<sup>2</sup> P. Lomax,<sup>2</sup> P.F. Griffin,<sup>1</sup> and E. Riis<sup>1</sup>

<sup>1</sup>*Department of Physics, SUPA, University of Strathclyde, Glasgow G4 0NG, UK*

<sup>2</sup>*Scottish Microelectronics Centre, University of Edinburgh, Edinburgh EH9 3FF, UK*

(\*Electronic mail: terry.dyer@strath.ac.uk)

(Dated: 3 November 2022)

Micro-fabricated vapour cells have applications in a number of emerging quantum technology based devices including miniaturized atomic magnetometers, atomic clocks and frequency references for laser systems. Increasing the cell optical path length (OPL) and smallest cell dimension is normally desirable to increase the signal to noise ratio (SNR) and minimize the de-polarization rate due to collisions between atomic or molecular species and the cell walls. This paper presents a fully wafer-level scalable fabrication process to manufacture vapour cells with dimensions approaching those of glass-blown cells. The fabrication process is described and spectroscopic measurements (optical absorption and magnetic resonance) are reported. A magnetic resonance linewidth of 350 Hz is demonstrated, this is the smallest linewidth reported to date for a micro-fabricated vapour cell.

## I. INTRODUCTION

One of the major advantages of micro-fabrication for vapour cell production is the ability to process many cells in parallel at the wafer level<sup>1-3</sup>. Leveraging semiconductor industry process control techniques can enable a high yield process resulting in significant economies of scale over glass-blown cells.

Glass-blown vapour cells are traditionally used in high performance atomic clocks, magnetometers and frequency references<sup>4,5</sup>. The first micro-fabricated vapour cells were developed using anisotropic wet etching of <100> silicon wafers<sup>6</sup>. More advanced techniques, such as deep reactive ion etching (DRIE), allowed the creation of increasingly complex cell geometries including interconnected reservoir/optical probe cells<sup>7</sup>. One downside of this approach is higher unit cost due in part to the reduced number of vapour cells per wafer. Both approaches require photolithography to define the vapour cell apertures prior to bulk silicon etching. The OPL of these vapour cells is set by the thickness of the silicon wafer. Unfortunately, thick silicon wafers can be difficult to source, require extended process times and are often incompatible with standard semiconductor processing equipment.

One approach<sup>8</sup> to increasing the OPL is to build an elongated cell along the silicon wafer surface plane. In our simpler approach, we use a thick BF33 glass wafer to set the OPL with apertures created by water-jet machining (recent work has also used this process to create apertures in a thick silicon wafer<sup>9</sup>). Water-jetting is an attractive method for fabricating vapour cells as the process is low-cost and does not require a clean room, photolithography is not required as the mask design file can be read directly by the water-jet tool.

TABLE I. Selected thermal properties of silicon and BF33 glass wafers<sup>10</sup>.

	silicon	BF33 glass
Thermal conductivity W/(m.K)	148	1.2
Specific heat capacity J/(kg.K)	700	830

There is also a vapour cell performance advantage especially for battery operated portable devices. The thermal conductivity of BF33 glass is lower than for silicon and its specific heat capacity is higher (Table 1). Therefore, a vapour cell fabricated principally from BF33 glass will have improved thermal stability over a silicon based vapour cell.

Low temperature silicon-glass anodic bonding<sup>11</sup> has dominated the development of micro-fabricated alkali vapour cells. It is used to form both bonds in the conventional glass-silicon-glass wafer stack and results in high hermeticity. Our approach uses a combination of fusion (direct) and anodic bonding to enable bonding of both glass-glass and silicon-glass wafers. Fusion bonding has not previously been reported in vapor cell fabrication, in part due to the stringent cleanliness and surface property requirements<sup>12</sup>. However, by designing the process flow such that fusion bonding occurs at the start of the process we can subcontract this step to a manufacturer with the necessary clean room infrastructure. This additional capability enables a novel vapour cell architecture with cell dimensions approaching those of glass-blown ones.

Finally, alkali metal can be introduced into the vapour cell using several methods<sup>13</sup>. We have selected aqueous CsN<sub>3</sub> dispense/UV activation<sup>14</sup> as it is low-cost and can be conveniently carried out using precision fluid dispensing robotic systems and 254 nm UV cross-linker exposure tools.

## II. VAPOUR CELL FABRICATION PROCESS

Micro-fabricated rubidium vapour cells with OPL = 4 mm have been reported previously using mechanical drilling of a glass wafer and a hybrid fabrication process requiring four anodic bonds<sup>15</sup>. Our entirely wafer-level fabrication process (Fig 1) uses water-jetting to form the glass cavity, extends the OPL to 5 mm and reduces the number of bonds required to two. Reducing the number of bonds is key to maintaining a low stress wafer stack and enables a fully wafer level process. Water jetting also results in smoother sidewalls compared to mechanical drilling. The water-jet process creates apertures in the glass wafer with near vertical sidewalls tapered by 3-5 deg. The aperture size tolerance is 0.1 mm and the minimum

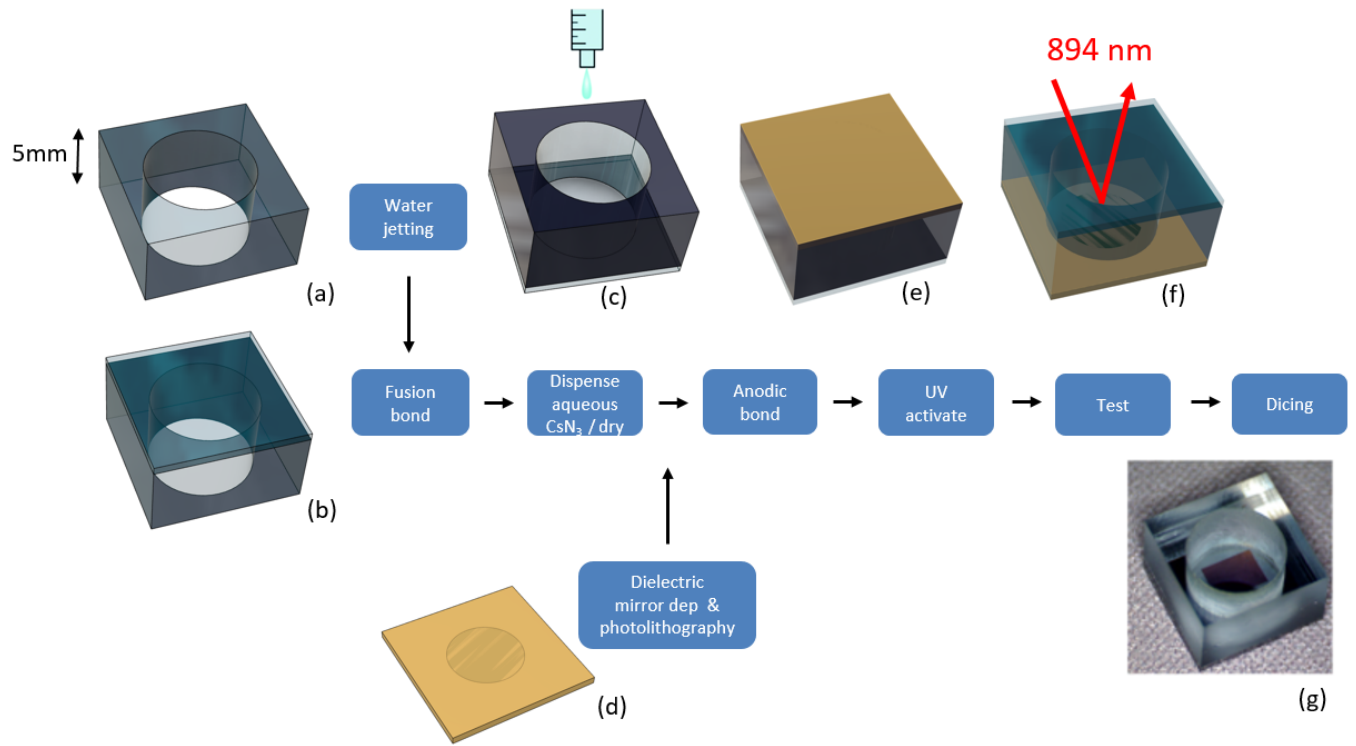


FIG. 1. Cell level illustration of the 150 mm wafer fabrication process (each wafer contains 120 cells). A 5 mm thick BF33 glass wafer is water-jet processed (a). One surface is then fusion bonded (b) to a 0.5 mm BF33 glass wafer. Aqueous  $\text{CsN}_3$  is dispensed into the open cavity (c) and dried in a controlled environment. A silicon wafer containing patterned dielectric mirrors (d) is then aligned and anodically bonded to the open glass cavity (e). UV activation of  $\text{CsN}_3$  is carried out to generate elemental Cs and  $\text{N}_2$ . Finally, cells are tested at the wafer level (f) before mechanical dicing (g).

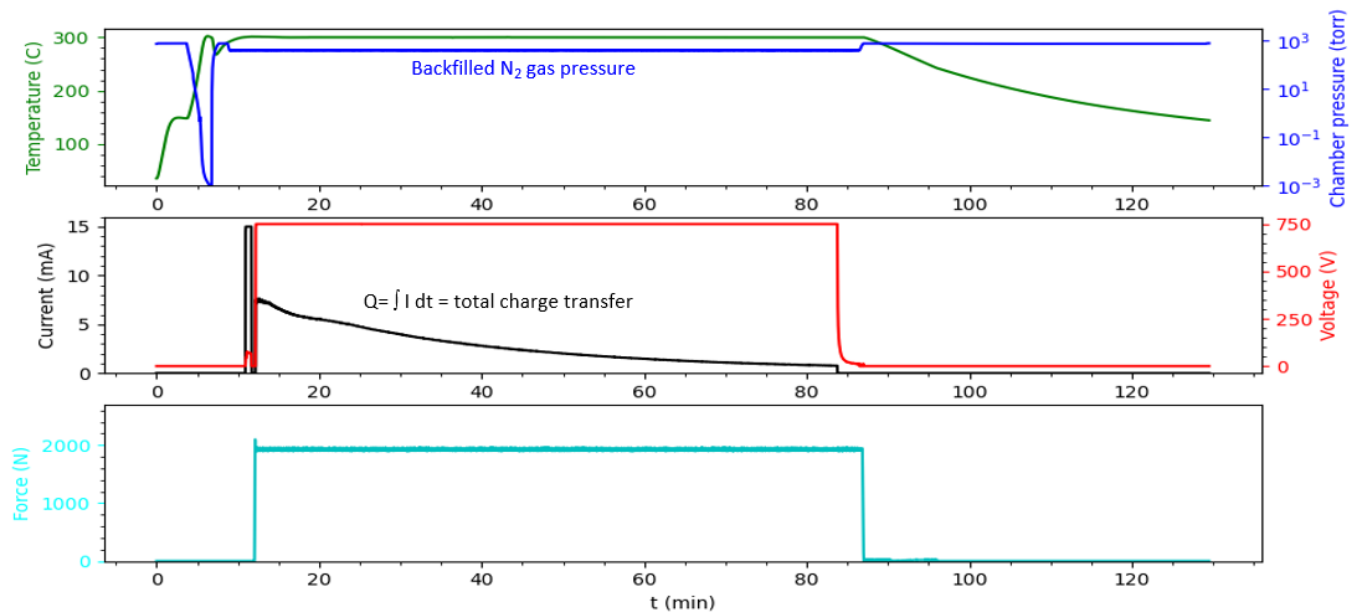


FIG. 2. Example of anodic bonding machine event sequence and process control (step (e) in Fig 1)). The 3 plots illustrate temperature, pressure, anodic bonding current and applied force as a function of elapsed process time. The backfilled  $\text{N}_2$  pressure is additive to the ( $\approx 10\times$  smaller)  $\text{N}_2$  pressure generated during the  $\text{CsN}_3$  UV activation process. The total charge transfer,  $Q$ , is a reliable indicator of the hermeticity of the anodic bond.

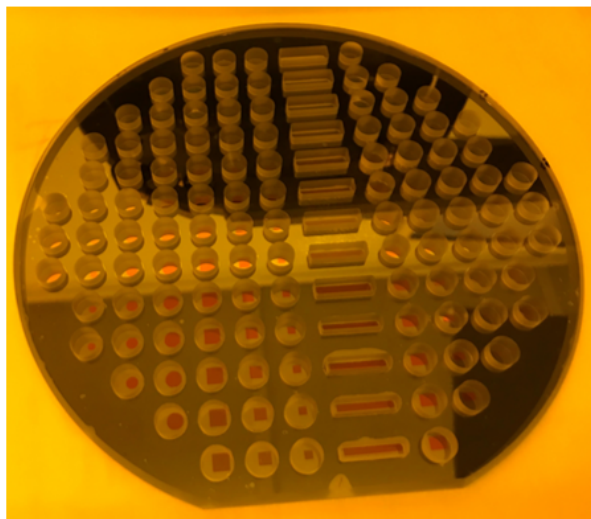


FIG. 3. Fully processed 150 mm wafer stack 6 mm thick containing 120 individual vapour cells with a range of aperture sizes and dielectric mirror configurations. The cell windows are clear of  $\text{CsN}_3$  crystal residue.

corner radius is  $\approx 0.5$  mm. This leads to a preferred circular or rounded square/rectangle aperture suitable for fabricating atomic vapour cells.

Optical access to the vapour cell is via the upper fusion bonded glass window, light is reflected from the lower anodic bonded Si wafer which contains a patterned dielectric mirror. The external vapour cell BF33 glass sidewall smoothness is determined by the mechanical dicing process and can be controlled to near optical quality. We are investigating polishing the rougher BF33 glass internal sidewall (Fig 1g), generated by the water-jetting process, to allow light beams to be directed through the vapour cell sidewalls. Our early results demonstrate that this surface can be polished to optical quality in a separate process step prior to fusion bonding.

An example of the level of process control required to ensure high yield is shown in Fig 2 for the case of anodic bonding. The vapour cell  $\text{N}_2$  buffer gas pressure can be set principally through pressure control of the backfilled  $\text{N}_2$  introduced into the chamber prior to bringing the two wafers into contact. Due to the safety requirement not to flip the open cavities after  $\text{CsN}_3$  dispense (Fig 1c), anodic bonding is carried out with the Si wafer uppermost and biased positively with respect to the grounded glass wafer stack. The molar concentration of  $\text{CsN}_3 = 20$  mM in DI water, the actual dispensed volume/cell depends on the cell volume. One concern with the aqueous  $\text{CsN}_3$  dispense/UV activation method is the presence of dried  $\text{CsN}_3$  crystals in the optical path of the vapour cell, leading to reduced optical transparency. Through careful control of the evaporation kinetics we ensure that the dried  $\text{CsN}_3$  crystals are located on the inner cell sidewalls (Figs 1(g), 3).

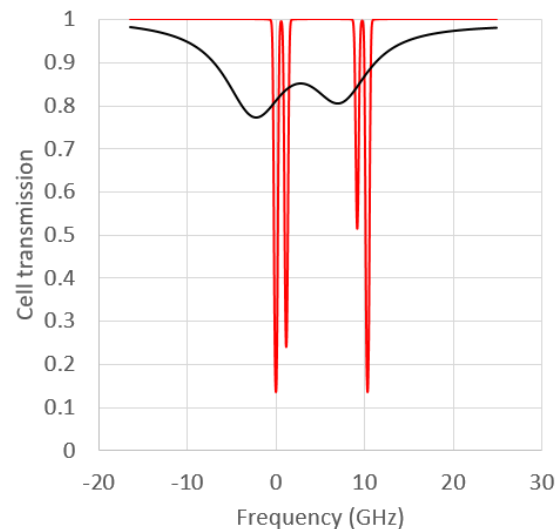


FIG. 4. Fitted transmission spectra for a 5 mm thick micro-fabricated caesium cell (black line) at 85 C and a caesium reference cell (red line). The frequency axis is scaled relative to the  $F_{\text{ground}=4} F_{\text{excited}=3}$  transition of the caesium D1 line.

### III. VAPOUR CELL CHARACTERISATION

#### A. Optical Absorption Spectroscopy

Optical absorption spectroscopy is carried out at wafer level to measure the pressure broadening due to  $\text{N}_2$  buffer gas. The 5mm micro-fabricated cells are probed by a double pass of a low intensity linearly polarised light beam. The laser intensity is maintained below the resonant saturation intensity  $I_{\text{sat}} = 25 \mu\text{W}\cdot\text{mm}^{-2}$  to avoid power broadening<sup>16</sup>. A reference setup was used to normalise the intensity variation of the laser and to provide a relative and absolute frequency reference.

Fig 4 illustrates the typical spectrum of a 5 mm micro-fabricated cell. The cell spectrum is both broadened and shifted with respect to the caesium reference cell spectrum. A cell pressure of 430 torr is estimated from a fit to a Voigt profile<sup>17</sup>, this value is in agreement with the targeted value. At this buffer gas pressure the four caesium D1 hyperfine transitions cannot be resolved and only two broadened transmission dips are observed.

Our optical absorption spectroscopy setup is coupled to a semi-automated wafer probe station with a heated chuck enabling wafer level cell testing. This approach is borrowed from the semiconductor industry and is key to enabling rapid testing and the “inking out” of cells outside specification that can be later discarded at the dicing stage. Fig 5 shows a wafer map for a fully processed 150 mm wafer. Each cell is labelled with its measured  $\text{N}_2$  pressure broadening value. Wafer maps containing other parametric parameters such as absorption, broadening and shift can be readily generated.



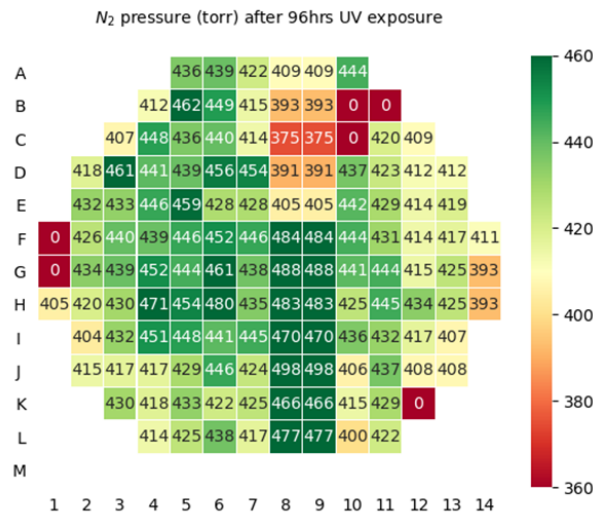


FIG. 5. Wafer map of vapour cell pressure broadening due to N<sub>2</sub> buffer gas across the 150 mm wafer stack in Fig 3. The functional yield is 95 % (cells labelled “0” are defective), average cell pressure is 432 torr with  $1\sigma = 22$  torr.

### B. Magnetic Resonance Spectroscopy

5 mm micro-fabricated cells have been successfully integrated into a portable double-resonance atomic magnetometer<sup>18</sup>. This is a single-beam magnetometer, avoiding any requirement for extensive optical hardware or full-field compensation. Magnetic resonance in atomic polarisation is detected using a polarimeter to measure optical rotation in transmitted pump light, allowing rejection of common-mode optical noise. We have fabricated wafers containing vapour cells at a range of different buffer gas pressures. Our initial characterisation results demonstrate a ground-state Cs spin decay rate of 350 Hz (excluding the effects of magnetic modulation saturation) calculated<sup>19</sup> from a fit to the data in Fig 6 from a cell with 200 torr N<sub>2</sub> buffer gas. This represents an  $\approx 3x$  improvement on previous work<sup>3</sup>. Future work will include characterisation of magnetic resonance linewidth vs buffer gas pressure.

## IV. CONCLUSIONS

We have developed a high-yield wafer level process for 5 mm OPL micro-fabricated caesium vapour cells and demonstrated magnetic resonance linewidth of 350 Hz from a cell with 200 torr N<sub>2</sub> buffer gas, this is the smallest linewidth reported to date for a micro-fabricated vapour cell. The process can be readily modified at the anodic bonding stage to target an N<sub>2</sub> buffer gas pressure over the range 50 1500 torr. Potential future work includes cell ageing studies, investigating different buffer gas compositions, alkali metals and the development of a fully fusion bonded micro-fabricated atomic vapour cell.

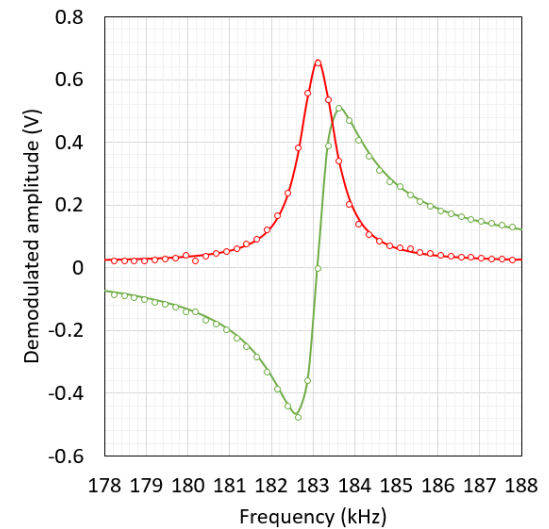


FIG. 6. In-phase and quadrature components of the magnetic resonance signal for an applied RF magnetic field that is swept through the Larmor frequency. The magnetic resonance linewidth is 350 Hz.

## ACKNOWLEDGMENTS

The authors would like to thank Dr Jonathan Pritchard for his work on the optical absorption spectroscopy setup. This work was funded in part by the UK Quantum Technology Hub in Sensing and Timing, EPSRC (Grant No EP/T001046/1).

## DATA AVAILABILITY STATEMENT

The data that support the findings of this study are openly available from the University of Strathclyde Knowledge-Base at <https://doi.org/10.15129/3ce0aa0f-7561-4997-a867-a89d6accf18c>.

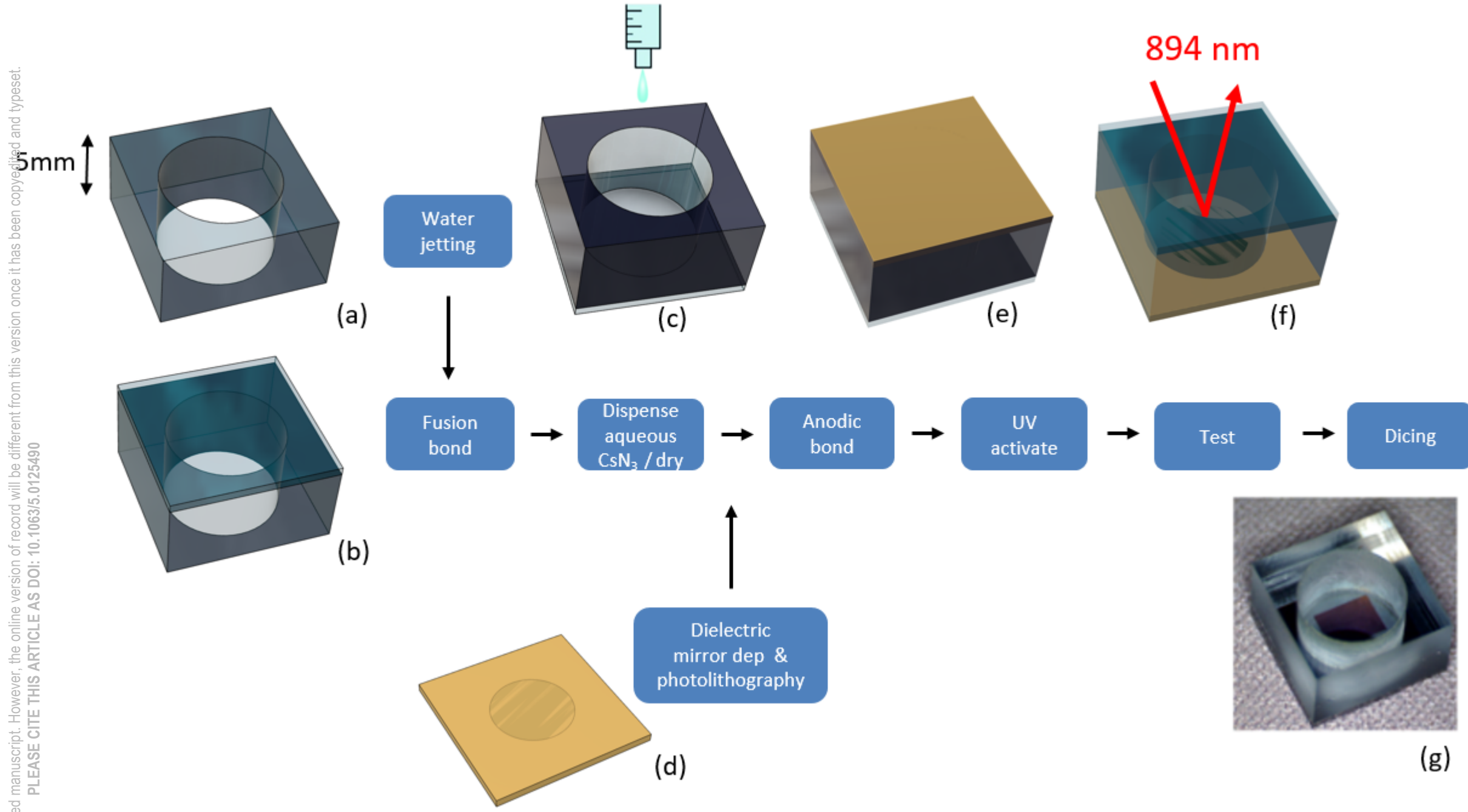
- <sup>1</sup>T. Overstolz, J. Haesler, and V. Spassov, U.S. Patent No. 8,906,470 B2 (9 Dec. 2014).
- <sup>2</sup>R. Vicarini, V. Maurice, M. Hafiz, J. Rutkowski, C. Gorecki, N. Passilly, L. Ribetto, V. Gaff, V. Volant, S. Galliou, and R. Boudot, “Demonstration of the mass-producible feature of a Cs vapor microcell technology for miniature atomic clocks,” *Sens. Act. A* **280**, 99 (2018).
- <sup>3</sup>R. Zhang, T. Dyer, N. Brockie, R. Parsa, and R. Mhaskar, “Subpicotesla scalar atomic magnetometer with a microfabricated cell,” *J. Appl. Phys.* **126**, 124503 (2019).
- <sup>4</sup>J. C. Allred, R. N. Lyman, T. Kornack, and M. Romalis, “High-sensitivity atomic magnetometer unaffected by spin-exchange relaxation,” *Phys. Rev. Lett* **89**, 130801 (2002).
- <sup>5</sup>E. J. Eklund, A. M. Shkel, S. Knappe, E. Donley, and J. Kitching, “Glass-blown spherical microcells for chip-scale atomic devices,” *Sensors. Actuators. A* **143**, 175 (2008).
- <sup>6</sup>L.-A. Liew, S. Knappe, J. Morland, H. Robinson, L. Hollberg, and J. Kitching, “Microfabricated alkali atom vapor cells,” *Appl. Phys. Lett.* **84**, 2694 (2004).
- <sup>7</sup>B. Bopp, V. Maurice, and J. Kitching, “Wafer-level fabrication of alkali vapor cells using in-situ atomic deposition atom vapor cells,” *J. Phys. Photonics.* **3**, 015002 (2021).
- <sup>8</sup>R. Chutani, V. Maurice, N. Passilly, C. Gorecki, R. Boudot, M. A. Hafiz, P. Abbé, S. Galliou, J.-Y. Rauch, and E. de Clercq, “Laser light routing in an elongated micromachined vapor cell with diffraction gratings for atomic clock applications,” *Scientific. Reports.* **5**, 14001 (2015).

This is the author's peer reviewed, accepted manuscript. However, the online version of record will be different from this version once it has been copyedited and typeset.

PLEASE CITE THIS ARTICLE AS DOI: 10.1063/5.0125490

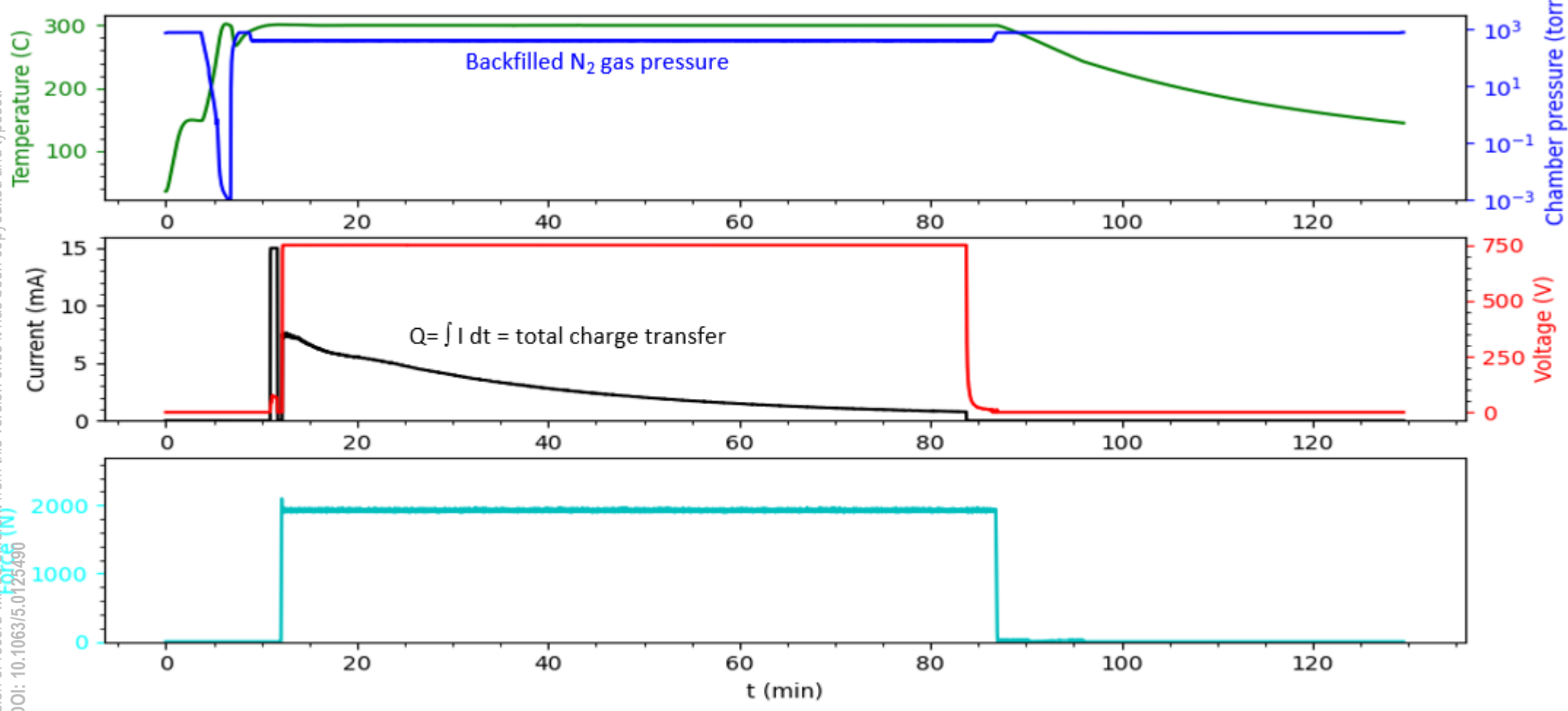
- <sup>9</sup>S. Dyer, P. F. Griffin, A. S. Arnold, F. Mirando, D. P. Burt, E. Riis, and J. P. McGilligan, "Micro-machined deep silicon atomic vapor cells," (2022), *J. Appl. Phys.* (accepted for publication).
- <sup>10</sup>D. Xia, L. Huang, L. Xu, and H. Gao, "Structural analysis of disk resonance gyroscope," *Micromachines* **8**, 296 (2017).
- <sup>11</sup>K. Malecki and F. G. D. Corte, "Silicon-glass anodic bonding at low temperature," *Proc. of SPIE*. **5715**, 180 (2005).
- <sup>12</sup>A. Plöbl and G. Kräuter, "Wafer direct bonding: tailoring adhesion between brittle materials," *Mat. Sci. and Eng.* **R25**, 1 (1999).
- <sup>13</sup>P. Knapkiewicz, "Technological assessment of MEMS alkali vapor cells for atomic references," *Micromachines* **10**, 25 (2018).
- <sup>14</sup>S. Woetzel, V. Schultze, R. IJsselsteijn, T. Schulz, S. Anders, R. Stolz, and H.-G. Meyer, "Microfabricated atomic vapor cell arrays for magnetic field measurements," *Rev. Sci. Instrum.* **82**, 033111 (2011).
- <sup>15</sup>Y. Pétremand, C. Affolderbach, R. Straessle, M. Pellaton, D. Briand, G. Mileti, and N. F. D. Rooij, "Microfabricated rubidium vapour cell with a thick glass core for small-scale atomic clock applications," *Rev. Sci. Instrum.* **22**, 025013 (2012).
- <sup>16</sup>D. Hunter, Ph.D. thesis, University of Strathclyde (2019).
- <sup>17</sup>G. A. Pitz, D. E. Wertepny, and G. P. Perram, "Pressure broadening and shift of the cesium D<sub>1</sub> transition by the noble gases and N<sub>2</sub>, H<sub>2</sub>, HD, D<sub>2</sub>, CH<sub>4</sub>, C<sub>2</sub>H<sub>6</sub>, CF<sub>4</sub>, and <sup>3</sup>He," *Physical. Review. A* **80**, 062718 (2009).
- <sup>18</sup>S. Ingleby, P. Griffin, T. Dyer, M. Mrozowski, and E. Riis, "A digital alkali spin maser," *Scientific. Reports.* **12**, 12888 (2022).
- <sup>19</sup>C. O'Dwyer, S. J. Ingleby, I. C. Chalmers, P. F. Griffin, and E. Riis, "A feed-forward measurement scheme for periodic noise suppression in atomic magnetometry," *Rev. Sci. Instrum.* **91**, 045103 (2020).

This is the author's peer reviewed, accepted manuscript. However, the online version of record will be different from this version once it has been copyedited and typeset. PLEASE CITE THIS ARTICLE AS DOI: 10.1063/5.0125490



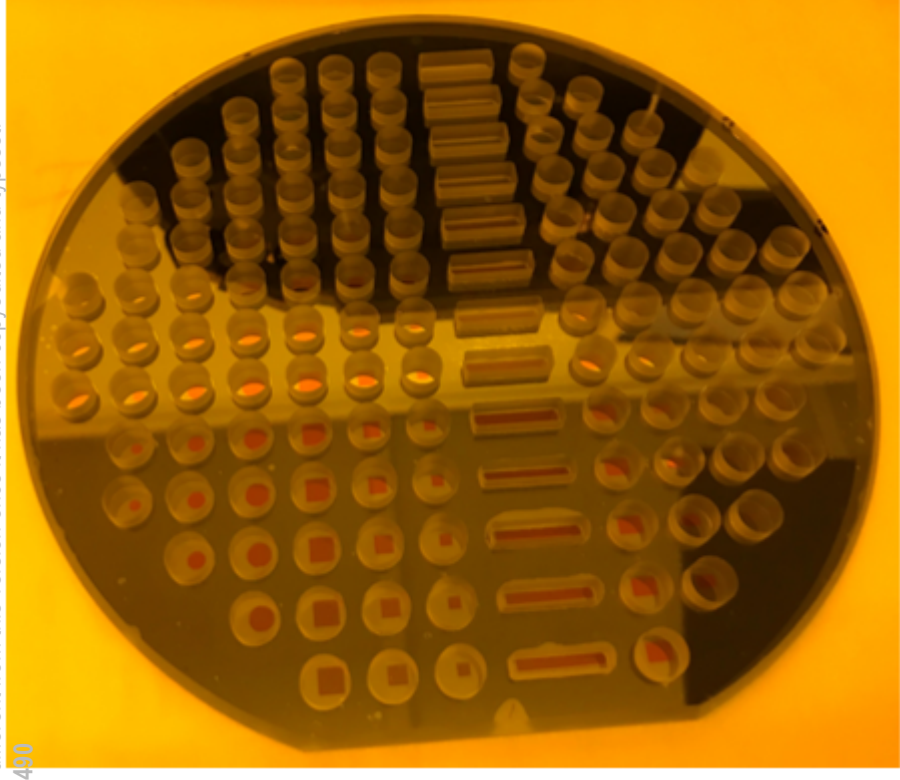
This is the author's peer reviewed, accepted manuscript. However, the online version of record will be different from this version once it has been copyedited and typeset.

PLEASE CITE THIS ARTICLE AS DOI: 10.1063/5.0125490

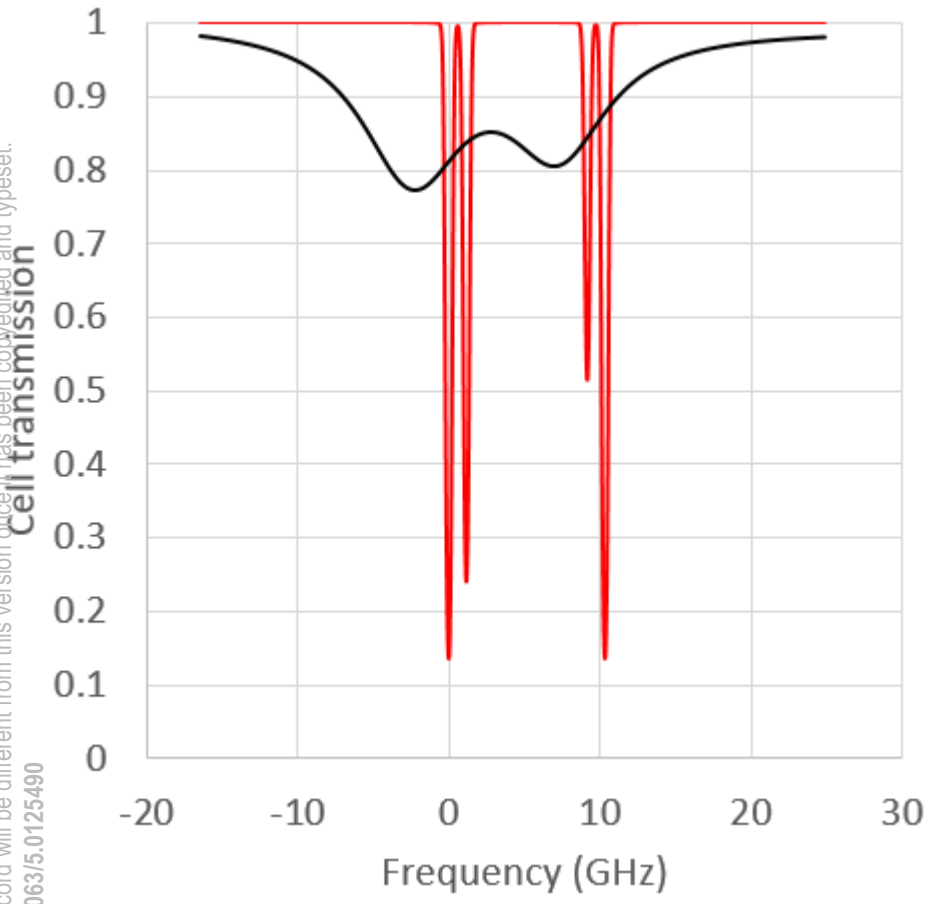




This is the author's peer reviewed, accepted manuscript. However, the online version of record will be different from this version once it has been copyedited and typeset.  
PLEASE CITE THIS ARTICLE AS DOI: 10.1063/5.0125440



This is the author's peer reviewed, accepted manuscript. However, the online version of record will be different from this version once it has been copyedited and typeset.  
PLEASE CITE THIS ARTICLE AS DOI: 10.1063/5.0125490





This is the author's peer reviewed, accepted manuscript. However, the online version of record will be different from this version once it has been copyedited and typeset.  
PLEASE CITE THIS ARTICLE AS DOI: 10.1063/5.0125490

**Demodulated amplitude (V)**

